THE JOURNAL OF PHYSICAL CHEMISTRY C

Article

Cite This: J. Phys. Chem. C 2018, 122, 19110−19115

pubs.acs.org/JPCC

Optical Absorption of Dye Molecules in a Spherical Shell Geometry

Baptiste Auguié*[,†,‡,¶] and Eric C. Le Ru[†,‡,¶]

[†]School of Chemical and Physical Sciences, Victoria University of Wellington, PO Box 600, Wellington 6140, New Zealand

[‡]The MacDiarmid Institute for Advanced Materials and Nanotechnology, PO Box 600, Wellington 6140, New Zealand

[¶]The Dodd-Walls Centre for Quantum and Photonic Technologies, PO Box 56, Dunedin 9054, New Zealand

Supporting Information

ABSTRACT: Dipole−dipole interactions between neighboring dye molecules can cause substantial spectral changes in optical absorption, with a strong dependence on near-neighbors' relative distances and orientations. Such effects have been previously investigated in dimers, as well as planar arrangements of dipoles, but not to our knowledge in a three-dimensional spherical configuration. This work provides a comprehensive exploration of the effect of dipolar interactions in such a geometry, varying the dye concentration, orientations, and uniformity in coverage. We also contrast this coupled-dipole model to a simpler but often-used homogeneous effective-medium approximation, which ignores effects of orientation and nonuniformity. The results provide a first step toward the full description of light scattering in a complex anisotropic core−shell geometry, which is of strong relevance in surface-enhanced spectroscopy applications, as well as in the strong coupling between molecular emitters and optical nanoresonators.

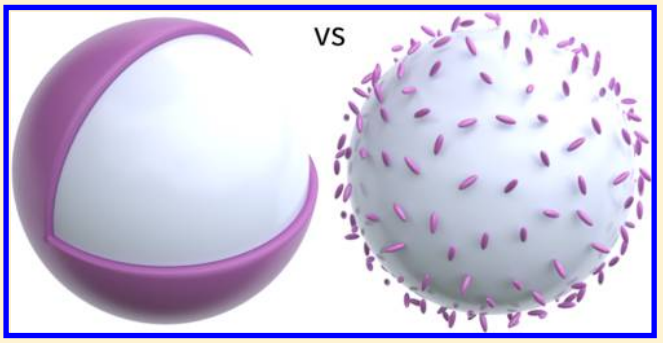

INTRODUCTION

Nanostructures and nanoparticles can substantially affect the absorption of light by vicinal molecules, raising considerable interest for such diverse applications as solar cells,[1−3] photochemistry,[4−7] plasmon-assisted Förster resonance energy transfer,[8,9] or surface-enhanced spectroscopies.[10] The topic is also of fundamental interest in quantum optics-related pursuits, such as strong coupling[11,12] or superradiance.[13] Recent experiments have demonstrated how optical absorption by dye molecules can be substantially modified upon adsorption on metal colloids, with some molecules experiencing an enhancement, a quenching, or a spectral modification of their absorption spectrum.[14] The variety of these effects likely has multiple physicochemical causes, some of which are explainable by classical electromagnetic theory. Comprehensive theoretical simulations are therefore required to disentangle the molecule-specific chemical interaction—in essence, changes to the intrinsic molecular response—from purely electromagnetic interactions due to the environment and the geometry of the light-scattering problem.

As a first step toward elucidating these electromagnetic effects, we apply a coupled-dipole model to describe the electromagnetic interaction between dye molecules arranged in a discrete spherical shell geometry. In experimental works, molecules are supported on a core nanoparticle (NP), and even within a purely electromagnetic framework, the optical response is affected by several factors: (i) dye−dye interactions, which depend on surface coverage and relative orientations, and (ii) dye−NP and NP-mediated dye−dye interactions, which may also affect the response of the core NP as the shell of dyes affects the local refractive index.[15] In this work, we focus on the first aspect and consider a hollow sphere of dyes, with homogeneous refractive index inside and outside (water). This model system allows us to disentangle the effects purely related to dye−dye interactions from those that are NP-related. While this constitutes a rather artificial model system, we note that an optically soft dielectric core such as a polymer or porous silica sphere[16] could be used as physical support for the shell of dye molecules, with only minor electromagnetic influence from the core particle.

Even in this simplified configuration, we predict a rich variety of spectral changes that depend on the relative orientation and distribution of dipoles on the spherical shell. This work therefore provides an essential starting point in understanding the full optical response of the coupled core−shell system.

RESULTS

Limitations of the Effective-Medium Shell Model. We first consider an effective-medium homogeneous shell model, representing the simplest approximation of a layer of molecules covering a spherical surface. This is the most common approach for theoretical studies of molecular layers on metallic nanoparticles.[17−24] We remark, however, that an empirical

Received: June 10, 2018
Revised: July 25, 2018
Published: August 6, 2018

DOI: 10.1021/acs.jpcc.8b05542
J. Phys. Chem. C 2018, 122, 19110−19115

expression for the wavelength-dependent dielectric function ε of an effective-medium shell is generally assumed, which precludes qualitative concentration-dependent predictions. Following ref 14, we instead introduce explicitly the local-field effects arising from the solvent (water) and dye molecules to derive an effective concentration-dependent dielectric function for the shell from the microscopic dye polarizability using the Clausius−Mossotti (CM) formula as detailed in the Supporting Information.

For simplicity, the polarizability of the dyes is described by a single Lorentzian function, which helps distinguish the concentration-induced spectral changes. The parameters are chosen to reproduce, for illustration, the main absorption spectrum of Rhodamine 6G (eq S6). More realistic polarizability prescriptions should be used for quantitative comparisons with experiments on molecular resonances,[25] but the interaction between multiple spectral features (multiple peaks and shoulders) tends to complicate the interpretation of apparent spectral shifts. In a typical experiment, the relevant parameter is the dye surface coverage ρ (number of adsorbed molecules per unit surface area), which can be derived from the NP concentration, NP surface area, dye concentration in solution, and adsorption efficiency. The volumetric dye concentration c_d in the effective-medium shell is therefore derived for a spherical shell of thickness d as $c_d \approx \rho/d$, or to be more precise, for a sphere of inner radius R as

$$c_d = \frac{3\rho R^2}{(R+d)^3 - R^3} \tag{1}$$

The effective thickness d is a priori a free parameter and could in principle be used to tune the strength of the dye−dye interaction effects through c_d. In previous concentration-independent uses of the effective shell model, the predictions are independent of d for $d \ll R$. This is also the case in our model but only in the low-coverage limit. We here assume a typical value of d = 1 nm, in line with ref 14. For a given dye concentration, the Clausius−Mossotti formula (eq S5) yields the effective-medium dielectric function (Figure 1a), and the optical properties of the spherical shell can then be computed using standard Mie theory codes for multilayered spheres.[10,26] The resulting absorption cross sections are presented in Figure 1b.

As described in ref 14, an increase in dye concentration induces a splitting of the absorption band into an intense red-shifted band and a weaker blue-shifted band. This prediction, based on a rigorous solution of the continuous electrodynamics problem, does not reveal explicitly the microscopic origin of such a splitting, even though it is strongly reminiscent of dipole−dipole interactions observed in molecular dimers. The progressive red-shift of the peak in the imaginary part of the dielectric function is a result of dipole−dipole interactions embedded in the CM formula, but without reference to a specific orientation or geometry. The blue-shifted band coincides with a zero of the real value of the shell's dielectric function and is therefore reminiscent of an epsilon-near-zero resonance,[27] where all dipoles oscillate in phase. For both features the continuous-medium description of the optical response provides only an indirect link to their microscopic origin, namely, the electromagnetic interaction between dyes. In contrast, we present in Figure 2a the absorption spectrum of a dimer of dyes, with the two molecules described by isotropic

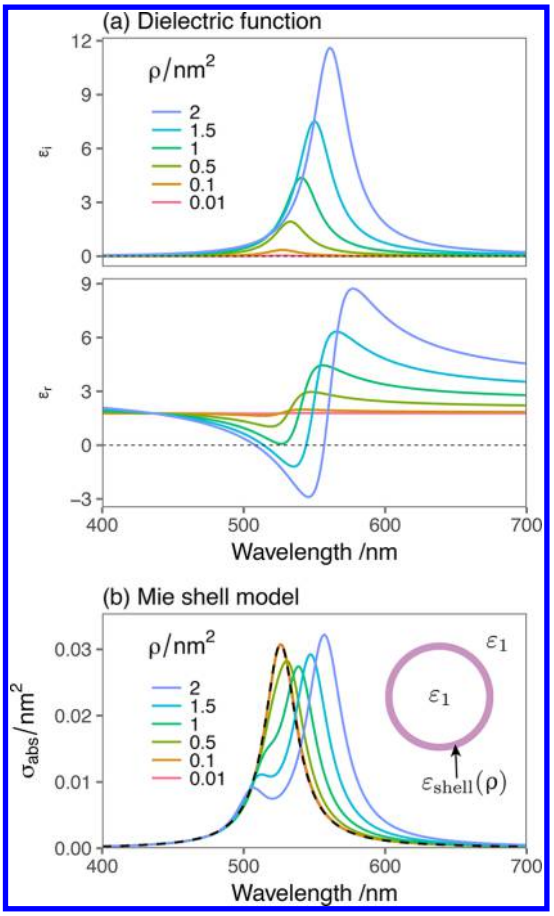

Figure 1. (a) Concentration-dependent dielectric function of a dye−water mixture for various dye concentrations (eq S5). The concentration c_d is related to the surface coverage ρ through eq 1, assuming a 1 nm thick shell. (b) Absorption spectra predicted by Mie theory for a homogeneous spherical shell of inner radius 14 nm and thickness 1 nm, with effective dielectric function as above. The absorption cross section is normalized by the number of molecules in the spherical shell. For small ρ, those results are independent of the choice of d (as long as $d \ll R$). The dashed line shows for reference the absorption spectrum of a single dye molecule in water, according to eqs S6 and S7.

polarizability tensors and their interaction explicitly described by a coupled-dipole model.[28−30]

The dimer configuration has been studied extensively,[31] as many dye molecules tend to dimerize at sufficiently high concentrations.[32] The resulting dimers are known as J- or H-aggregates, depending on the relative orientation of the two interacting dipoles. With decreasing separation, the molecular resonances interact and hybridize; the spectral line shape exhibits a red-shift (Figure 2a, left panel) or a blue-shift (right panel) according to the respective orientation of the induced dipole moments (head-to-tail and side-by-side, respectively). The difference between these two configurations is purely geometrical; accordingly, a spherical shell excited by an incident plane wave will generally present a mixture of both types of dipole−dipole interaction, i.e. side-by-side where the incident field is normal to the spherical shell and head-to-tail where it is tangential.

Figures 1b and 2a highlight the necessity to extend the theoretical description of dye shells beyond that of a homogeneous effective-medium layer, to address explicitly

DOI: 10.1021/acs.jpcc.8b05542
J. Phys. Chem. C 2018, 122, 19110−19115

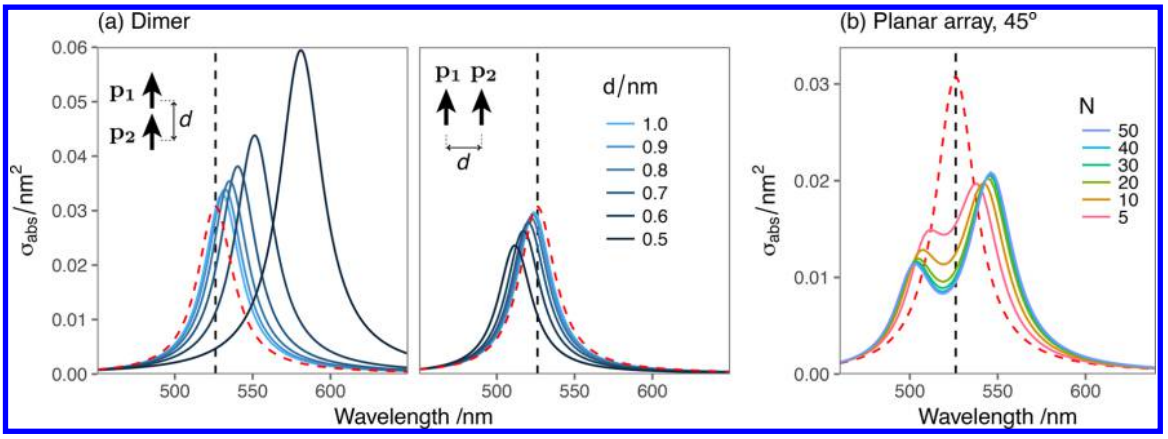

Figure 2. (a) Simulated absorption spectra for a dimer of dipoles with varying interdipole separation d. Light is incident normal to the dimer axis, with electric field parallel to the dipoles, which are placed "head-to-tail" (left) or "side-by-side" (right). (b) Absorption of a planar square array of $N \times N$ isotropic dipoles with constant surface density $\rho = 1.5$ nm^{-2}, with an incidence angle of 45° and TM polarization. The dashed red line is the absorbance of a single isolated dipole, for reference. The dye polarizability is given in eq S6. All spectra are normalized by the number of dipoles.

the dipole−dipole interactions between multiple dye molecules arranged in arbitrary positions and orientations. We note that even though a dimer model captures the essential physics of the spectral changes, an accurate prediction of spectral lineshapes as a function of surface coverage for nanoshells of subwavelength dimensions requires an explicit account of the exact position and orientation of all the dipoles in the simulation, allowed to interact via their self-consistent scattered field.[30] To illustrate this point, we present in Figure 2b the simulated absorption spectrum of a planar square array of $N \times N$ dye molecules with isotropic polarizabilities, with N ranging from 5 to 50, and a fixed surface density $\rho = 1.5$ nm^{-2}. The light is incident at 45° with TM (p) polarization, therefore exciting a mixture of head-to-tail and side-by-side interactions between nearest neighbors. We note that although this particular choice of polarization and angle of incidence is arbitrary, it illustrates the general case of coupling between arbitrarily oriented neighboring dipoles, in contrast to the more restricted case of TE polarization, or normal incidence. It is remarkable that a large number of dipoles are interacting with each other, as witnessed by the slow convergence of the spectra (all normalized to the number of dipoles). This is especially relevant for the blue-shifted mode which originates from side-by-side coupling: the dipolar field along such directions (in-plane) is able to collectively couple dipoles over large distances, as it contains a mixture of near-field and far-field components.[33,34]

The main purpose of this work is to clearly expose the microscopic origin of these spectral features observed in a spherical shell geometry, using a microscopic description of the dipole−dipole interactions between molecules, possibly with preferential orientations.

Shells of Point Dipoles. In what follows we consider N polarizable molecules organized as a spherical shell of radius R; the response of each molecule is described by a polarizability tensor α to allow anisotropic responses. In the coupled dipole model, the position and orientation of each molecule can be varied independently; for clarity, we will focus on a few specific configurations that provide a representative overview of the coupling between molecules in realistic configurations. We also chose to average the absorption cross sections over all directions of incidence and polarization in the following simulations, as the discrete number of dipoles breaks the spherical symmetry and small differences in optical response can arise for different directions of incidence.

Isotropic Response. We first compare the effective-medium and coupled-dipole models in Figure 3. Isotropic point dipoles were positioned regularly around a sphere according to a Fibonacci lattice,[35] providing near-homogeneous surface coverage (Figure 3b). In this configuration, we observe a close qualitative agreement with the predictions of the homogeneous shell model (Figure 3a). It should however be noted that the results are not exactly identical, except for the lowest concentrations. This is expected because the effective-medium model of eq S1 implicitly assumes a 3-dimensional averaging of neighboring dipoles homogeneously distributed in a bulk medium, while the coupled-dipole model explicitly considers the discrete set of pairwise distances between all dipoles in a finite spherical lattice. As noted in the previous section, the shell thickness d in the effective-medium model is required to provide a volume concentration for a known number of dipoles; this parameter was set arbitrarily to 1 nm, noting that a better match can be obtained at a given concentration by treating d as a free parameter. The effect of d on the predicted spectral shift in the effective-medium model is assessed against the coupled-dipole results in the Supporting Information. Regardless of the exact value of d chosen in the effective-medium model, in the limit of low concentrations, the results agree with the coupled-dipole model, and the absorption spectrum coincides with the spectrum of a dye in solution, scaled by the number of dipoles (see the Supporting Information for additional details). The coupled-dipole model thus provides a semiempirical guide to develop a more accurate effective-medium shell model, which is however beyond the scope of the present communication. We note that a rigorous description will necessarily lead to an anisotropic dielectric function, even for isotropic molecular polarizabilities, due to the anisotropic geometrical arrangement of dipoles.[36] We note that the treatment given in ref 37 only takes the assumption of isotropy in ε in order to simplify the formulas for this special case. No rigorous justification can be found for this choice, and indeed, in the general case one should expect an anisotropic dielectric function due to the structure factor's asymmetry parallel or normal to the plane of dipoles.

The surface coverage of a spherical nanoparticle is likely to be inhomogeneous in many practical cases; molecules may

DOI: 10.1021/acs.jpcc.8b05542
J. Phys. Chem. C 2018, 122, 19110−19115

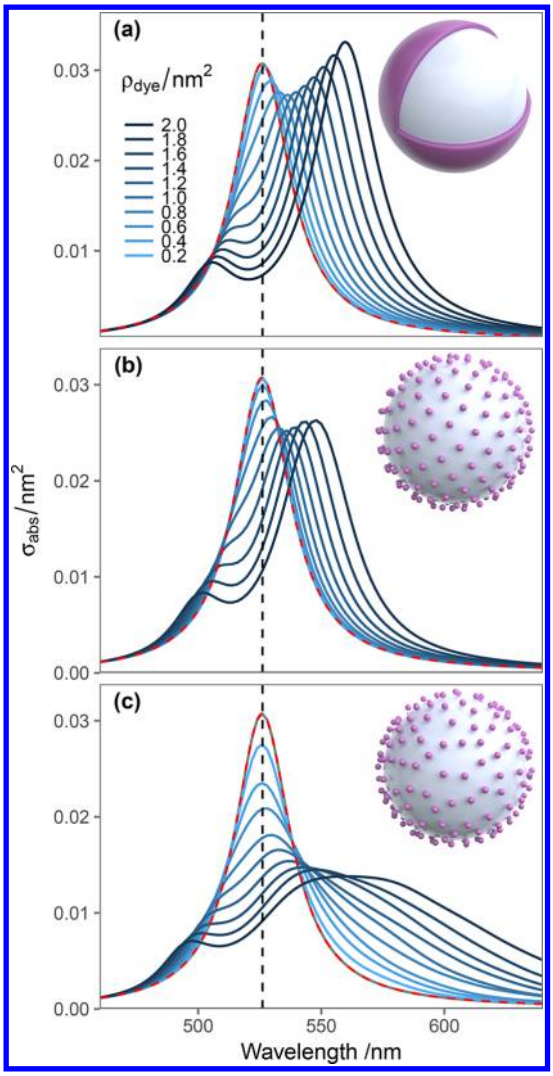

Figure 3. Predicted absorption spectra normalized by the number of dipoles for (a) a homogeneous shell described with Mie theory with d = 1 nm, (b) a homogeneous distribution of isotropic point dipoles, and (c) a random distribution of dipoles with a 0.5 nm minimal exclusion zone. In each panel the orientation-averaged single-molecule absorption spectrum is shown in dashed red curve for reference and coincides with the low-concentration limit $\rho_{dye} \to 0$ of both models.

adsorb at random positions on the surface, but they may also experience surface diffusion, repulsive or attractive forces, that will result in various degrees of inhomogeneity. To assess this effect on dipole−dipole interactions, we introduce in Figure 3c a more disordered coverage obtained by picking points at random on a sphere, with a minimal near-neighbor separation of 0.5 nm. This exclusion radius is necessary as two point dipoles arbitrarily close to each other would produce unphysical spectra (in reality, molecules cannot physically overlap; additionally, below a certain distance the electromagnetic interaction is no longer correctly described by a simple point dipole model). This comparison reveals that inhomogeneity in surface coverage yields qualitatively similar spectra, but with broader spectral features. Such spectral broadening is expected and follows from the range of near-neighbor interdipole separations introduced by disorder: the dipole−dipole interactions are convolved with a distribution of distances.

The results are presented for a specific shell radius of 15 nm, a size relevant to experiments on subwavelength nanoparticles. The radius of the shell impacts the relative position and orientation of neighboring dipoles, but comprehensive simulations showed that the effect is relatively minor in the range $10 \lesssim R \lesssim 50$ nm (further details are presented in the Supporting Information). The simulated spectra change rapidly below 10 nm in shell radius, as more and more dipoles are in such close proximity that they can interact beyond their nearest-neighbors, and the collective response approaches that of a spherical ball where, perhaps counterintuitively, the net effect of local-field corrections weakens because of symmetry.[38]

Orientation Effects. The coupled-dipole model allows us to consider orientation effects, using polarizability tensors that describe uniaxial molecules with a preferential orientation with respect to the spherical surface. In a real experiment, molecules would adsorb onto a spherical core, where the molecule−surface orientation may be affected, and sometimes controlled, by various factors such as surface charge, pH, functional groups, or co-ions.[39] For instance, studies have shown that the dye Nile blue adsorbs preferentially flat on a gold surface.[40]

We focus for simplicity on three specific cases of interest, varying the orientation of uniaxial tensors to represent idealized but experimentally relevant situations: an isotropic response, as in Figure 3; a uniaxial dipole with radial orientation; and a molecule with a tendency to align tangentially on the sphere, modeled as a uniaxial dipole with random orientation in the tangential plane. In all cases we enforce that the principal polarizability matrix elements be scaled to maintain an equal trace, for a meaningful comparison at constant total oscillator strength. Specifically, isotropic tensors are of the form $\alpha = \begin{pmatrix} \alpha_d & 0 & 0 \\ 0 & \alpha_d & 0 \\ 0 & 0 & \alpha_d \end{pmatrix}$ and uniaxial tensors $\alpha = \begin{pmatrix} 0 & 0 & 0 \\ 0 & 0 & 0 \\ 0 & 0 & 3\alpha_d \end{pmatrix}$ in the local frame of the dye molecule, with α_d the effective polarizability defined in the Supporting Information, such as only the directionality of the molecular response is varied with the anisotropy. These configurations are depicted schematically with ellipsoids oriented along the principal axis of α (insets of Figure 4).

The spherical geometry introduces a mixture of relative orientations between induced dipoles. With uniaxial-radial orientations (Figure 4b), the nearest neighbors are almost parallel to each other, resulting predominantly in side-by-side dipole−dipole interactions. In contrast, the in-plane uniaxial tensors corresponding to molecules adsorbed flat on a spherical core will see nearest-neighbor induced dipoles interacting predominantly head-to-tail (Figure 4c), as this near-field coupling is stronger by a factor of 2 for a given dipole separation. These interactions are reflected in the shifts of the spectra, which follow qualitatively those predicted for two interacting dipoles. However, the observed shifts are more pronounced in the spherical shell than from the pairwise interactions at a comparable dipole separation, and the predicted spectra are broader. This is most evident in the tangentially oriented configuration, where the random in-plane orientation of each dipole gives rise to a broad distribution of spectral shifts (mostly red-shifts), depending on the exact angle between any two dipoles. Furthermore, the uniaxial dipoles yield stronger dipole−dipole interactions, and therefore larger

DOI: 10.1021/acs.jpcc.8b05542
J. Phys. Chem. C 2018, 122, 19110−19115

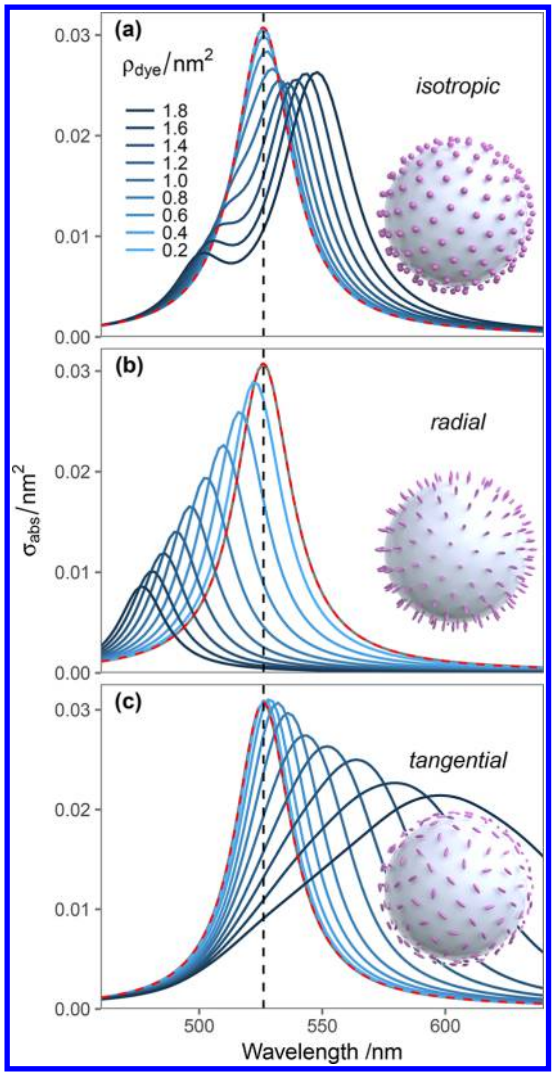

Figure 4. Orientation effects in dipole−dipole interactions between molecules. Concentration-dependent absorption spectra for a homogeneously covered shell of isotropic point dipoles described by (a) an isotropic tensor, (b) uniaxial polarizability tensors pointing radially, and (c) uniaxial tensors oriented randomly in the tangential plane (corresponding to a uniaxial molecule lying flat on the surface).

shifts, than isotropic dipoles because of our choice of normalization for the matrix elements.

CONCLUSIONS

The electromagnetic coupling between dye molecules arranged on a spherical shell of subwavelength dimensions displays a rich interaction between geometry and light polarization effects. Where a dimer can already present perturbations of a molecular absorption spectral line and lead to blue-shifts or red-shifts depending on the relative orientation of the induced dipole moments, the spherical geometries considered here sustain a nontrivial combination of both types of coupling. Through comprehensive numerical simulations, we highlighted the differences between a homogeneous, effective-medium description of a molecular shell and a more accurate description with discrete point dipoles. The importance of orientation effects and inhomogeneities in coverage could justify the development of a more accurate effective-medium theory for thin spherical shells, introducing anisotropy in the shell response[41] but also extending the Clausius−Mossotti formula to a spherical shell.[37,42,43] The coupled-dipole model described here will provide a very valuable comparison for such theories. We also note that the orientation of molecular dipoles has critical implications for all surface-enhanced spectroscopies through surface-selection rules in surface-enhanced Raman spectroscopy[40] and also in the context of optical activity.[44]

The natural extension of this work will consider the inclusion of a core particle sustaining the shell of dyes. The results described in the present work will provide a useful comparison to interpret the more complex spectral changes, as will be discussed elsewhere. The coupling between dipoles contains additional terms accounting for multipolar scattering by the core particle, which in the case of metal colloids may dramatically alter the near-field intensity and polarization. We note that such additions to the model are not trivial to include, as the electromagnetic solution for a dipolar emitter close to a sphere[45] involves series that can be ill-suited for efficient numerical implementation.[46]

ASSOCIATED CONTENT

Supporting Information

The Supporting Information is available free of charge on the ACS Publications website at DOI: 10.1021/acs.jpcc.8b05542.

Effective medium dielectric function for dyes in a solvent; model comparison in the low-concentration limit; brief summary of the coupled dipole equations; consistency of results with random orientations; shell radius dependence of the predicted spectra.(PDF)

AUTHOR INFORMATION

Corresponding Author

*E-mail: baptiste.auguie@vuw.ac.nz.

ORCID

Baptiste Auguié: 0000-0002-2749-5715

Eric C. Le Ru: 0000-0002-3052-9947

Author Contributions

B.A. and E.C.L.R. jointly conceived the study and wrote the computer code. B.A. performed all numerical simulations. Interpretation of the results and the writing of the manuscript was also a joint effort.

Notes

The authors declare no competing financial interest.

ACKNOWLEDGMENTS

The authors thank the Royal Society Te Apārangi for support through a Rutherford Discovery Fellowship (B.A.) and a Marsden grant (E.C.L.R.).

REFERENCES

(1) Atwater, H. A.; Polman, A. Plasmonics for improved photovoltaic devices. *Nat. Mater.* **2010**, *9*, 205−213.

(2) Linic, S.; Christopher, P.; Ingram, D. B. Plasmonic-metal nanostructures for efficient conversion of solar to chemical energy. *Nat. Mater.* **2011**, *10*, 911−921.

(3) Jang, Y. H.; Jang, Y. J.; Kim, S.; Quan, L. N.; Chung, K.; Kim, D. H. Plasmonic solar cells: from rational design to mechanism overview. *Chem. Rev.* **2016**, *116*, 14982−15034.

(4) Kleinman, S. L.; Frontiera, R. R.; Henry, A.-I.; Dieringer, J. A.; Van Duyne, R. P. Creating, characterizing, and controlling chemistry with SERS hot spots. *Phys. Chem. Chem. Phys.* **2013**, *15*, 21−36.

DOI: 10.1021/acs.jpcc.8b05542
J. Phys. Chem. C 2018, 122, 19110−19115

(5) Xu, S.; Shan, J.; Shi, W.; Liu, L.; Xu, L. Modifying photoisomerization efficiency by metallic nanostructures. *Opt. Express* **2011**, *19*, 12336.
(6) Galloway, C. M.; Artur, C.; Grand, J.; Le Ru, E. C. Photobleaching of fluorophores on the surface of nanoantennas. *J. Phys. Chem. C* **2014**, *118*, 28820−28830.
(7) Zhang, Y.; He, S.; Guo, W.; Hu, Y.; Huang, J.; Mulcahy, J. R.; Wei, W. D. Surface-plasmon-driven hot electron photochemistry. *Chem. Rev.* **2018**, *118*, 2927.
(8) Zhao, L.; Ming, T.; Shao, L.; Chen, H.; Wang, J. Plasmon-controlled Förster resonance energy transfer. *J. Phys. Chem. C* **2012**, *116*, 8287−8296.
(9) Bidault, S.; Devilez, A.; Ghenuche, P.; Stout, B.; Bonod, N.; Wenger, J. Competition between Förster resonance energy transfer and donor photodynamics in plasmonic dimer nanoantennas. *ACS Photonics* **2016**, *3*, 895−903.
(10) Le Ru, E. C.; Etchegoin, P. G. *Principles of surface enhanced Raman spectroscopy and related plasmonic effects*; Elsevier: Amsterdam, 2009.
(11) Törmä, P.; Barnes, W. L. Strong coupling between surface plasmon polaritons and emitters. *Rep. Prog. Phys.* **2015**, *78*, 013901.
(12) Chikkaraddy, R.; de Nijs, B.; Benz, F.; Barrow, S. J.; Scherman, O. A.; Rosta, E.; Demetriadou, A.; Fox, P.; Hess, O.; Baumberg, J. J. Single-molecule strong coupling at room temperature in plasmonic nanocavities. *Nature* **2016**, *535*, 127−130.
(13) Fauché, P.; Kosionis, S. G.; Lalanne, P. Collective scattering in hybrid nanostructures with many atomic oscillators coupled to an electromagnetic resonance. *Phys. Rev. B: Condens. Matter Mater. Phys.* **2017**, *95*. DOI: 10.1103/PhysRevB.95.195418
(14) Darby, B. L.; Auguié, B.; Meyer, M.; Pantoja, A. E.; Le Ru, E. C. Modified optical absorption of molecules on metallic nanoparticles at sub-monolayer coverage. *Nat. Photonics* **2016**, *10*, 40−45.
(15) Haes, A. J.; Zou, S.; Zhao, J.; Schatz, G. C.; Van Duyne, R. P. Localized surface plasmon resonance spectroscopy near molecular resonances. *J. Am. Chem. Soc.* **2006**, *128*, 10905−10914.
(16) Zou, H.; Schlaad, H. Thermoresponsive PNIPAM/silica nanoparticles by direct photopolymerization in aqueous media. *J. Polym. Sci., Part A: Polym. Chem.* **2015**, *53*, 1260−1267.
(17) Wiederrecht, G. P.; Wurtz, G. A.; Hranisavljevic, J. Coherent coupling of molecular excitons to electronic polarizations of noble metal nanoparticles. *Nano Lett.* **2004**, *4*, 2121−2125.
(18) Fofang, N. T.; Park, T.-H.; Neumann, O.; Mirin, N. A.; Nordlander, P.; Halas, N. J. Plexcitonic nanoparticles: Plasmon-exciton coupling in nanoshell-J-aggregate complexes. *Nano Lett.* **2008**, *8*, 3481−3487.
(19) Ni, W.; Ambjörnsson, T.; Apell, S. P.; Chen, H.; Wang, J. Observing plasmonic-molecular resonance coupling on single gold nanorods. *Nano Lett.* **2010**, *10*, 77−84.
(20) Chen, H.; Shao, L.; Woo, K. C.; Wang, J.; Lin, H.-Q. Plasmonic-molecular resonance coupling: plasmonic splitting versus energy transfer. *J. Phys. Chem. C* **2012**, *116*, 14088−14095.
(21) Zengin, G.; Johansson, G.; Johansson, P.; Antosiewicz, T. J.; Käll, M.; Shegai, T. Approaching the strong coupling limit in single plasmonic nanorods interacting with J-aggregates. *Sci. Rep.* **2013**, *3*, 3074.
(22) Schlather, A. E.; Large, N.; Urban, A. S.; Nordlander, P.; Halas, N. J. Near-field mediated plexcitonic coupling and giant Rabi splitting in individual metallic dimers. *Nano Lett.* **2013**, *13*, 3281−3286.
(23) Antosiewicz, T. J.; Apell, S. P.; Shegai, T. Plasmon-exciton interactions in a core-shell geometry: From enhanced absorption to strong coupling. *ACS Photonics* **2014**, *1*, 454−463.
(24) Cacciola, A.; Di Stefano, O.; Stassi, R.; Saija, R.; Savasta, S. Ultrastrong coupling of plasmons and excitons in a nanoshell. *ACS Nano* **2014**, *8*, 11483−11492.
(25) Djorović, A.; Meyer, M.; Darby, B. L.; Le Ru, E. C. Accurate modeling of the polarizability of dyes for electromagnetic calculations. *ACS Omega* **2017**, *2*, 1804−1811.
(26) Le Ru, E. C.; Etchegoin, P. G. SERS and Plasmonics Codes (SPlaC). Matlab codes freely available from http://www.vuw.ac.nz/raman/book/codes.aspx, 2009.
(27) Engheta, N. Pursuing near-zero response. *Science* **2013**, *340*, 286−287.
(28) DeVoe, H. Optical properties of molecular aggregates. I. classical model of electronic absorption and refraction. *J. Chem. Phys.* **1964**, *41*, 393−400.
(29) Purcell, E. M.; Pennypacker, C. R. Scattering and absorption of light by nonspherical dielectric grains. *Astrophys. J.* **1973**, *186*, 705−714.
(30) Keller, D.; Bustamante, C. Theory of the interaction of light with large inhomogeneous molecular aggregates. I. Absorption. *J. Chem. Phys.* **1986**, *84*, 2961−2971.
(31) Kasha, M.; Rawls, H. R.; Ashraf, E.-B. M. The exciton model in molecular spectroscopy. *Pure Appl. Chem.* **1965**, *11*, 371−392.
(32) Ohno, H.; Taniguchi, K.; Fujita, K. Polarized optical waveguide spectroscopy: Effective tool to analyze adsorption process of dye molecules. *Opt. Rev.* **2009**, *16*, 233−240.
(33) García de Abajo, F. J. Colloquium: Light scattering by particle and hole arrays. *Rev. Mod. Phys.* **2007**, *79*, 1267−1290.
(34) Novotny, L.; Hecht, B. *Principles of nano-optics*; Cambridge University Press: Cambridge, 2006.
(35) Hannay, J. H.; Nye, J. F. Fibonacci numerical integration on a sphere. *J. Phys. A: Math. Gen.* **2004**, *37*, 11591.
(36) Collin, R. E. *Field theory of guided waves*; Wiley-IEEE Press, 1991; p 864.
(37) Dignam, M. J.; Moskovits, M. Optical properties of sub-monolayer molecular films. *J. Chem. Soc., Faraday Trans. 2* **1973**, *69*, 56−64.
(38) Markel, V. A. Introduction to the Maxwell Garnett approximation: tutorial. *J. Opt. Soc. Am. A* **2016**, *33*, 1244−1256.
(39) Hildebrandt, P.; Stockburger, M. Surface-enhanced resonance Raman spectroscopy of Rhodamine 6G adsorbed on colloidal silver. *J. Phys. Chem.* **1984**, *88*, 5935−5944.
(40) Le Ru, E. C.; Meyer, S. A.; Artur, C.; Etchegoin, P. G.; Grand, J.; Lang, P.; Maurel, F. Experimental demonstration of surface selection rules for SERS on flat metallic surfaces. *Chem. Commun.* **2011**, *47*, 3903.
(41) Roth, J.; Dignam, M. J. Scattering and extinction cross sections for a spherical particle coated with an oriented molecular layer. *J. Opt. Soc. Am.* **1973**, *63*, 308−311.
(42) Aspnes, D. E. Local-field effects and effective-medium theory: A microscopic perspective. *Am. J. Phys.* **1982**, *50*, 704−709.
(43) Markel, V. A. Maxwell Garnett approximation (advanced topics): tutorial. *J. Opt. Soc. Am. A* **2016**, *33*, 2237−2255.
(44) Keller, D.; Bustamante, C. Theory of the interaction of light with large inhomogeneous molecular aggregates. II. Psi-type circular dichroism. *J. Chem. Phys.* **1986**, *84*, 2972−2980.
(45) Chew, H. Transition rates of atoms near spherical surfaces. *J. Chem. Phys.* **1987**, *87*, 1355−1360.
(46) Majić, M. R.; Auguié, B.; Le Ru, E. C. Spheroidal harmonic expansions for the solution of Laplace's equation for a point source near a sphere. *Phys. Rev. E: Stat. Phys., Plasmas, Fluids, Relat. Interdiscip. Top.* **2017**, *95*, 033307.

DOI: 10.1021/acs.jpcc.8b05542
J. Phys. Chem. C 2018, 122, 19110−19115

Supporting Information for:

Optical absorption of dye molecules in a spherical shell geometry

Baptiste Auguié*,†,‡,¶ and Eric C. Le Ru†,‡,¶

†*School of Chemical and Physical Sciences, Victoria University of Wellington, PO Box 600, Wellington, New Zealand*

‡*The MacDiarmid Institute for Advanced Materials and Nanotechnology*

¶*The Dodd-Walls Centre for Quantum and Photonic Technologies*

E-mail: baptiste.auguie@vuw.ac.nz

Contents

A Effective medium dielectric function

A.1 Clausius-Mossotti formula for dyes in a solvent

The Clausius-Mossotti (CM) equation relates the molecular polarisability to the dielectric function ε of a bulk material[1,2] as

$$\frac{\varepsilon - 1}{\varepsilon + 2} = \sum_i \bar{\alpha}_i \tag{S1}$$

where we define the normalised polarisability of species i as $\bar{\alpha}_i = c_i \frac{\alpha_i}{3\varepsilon_0}$, with c_i the species' concentration in m^{-3}, and $\varepsilon_0 = 8.854 \times 10^{-12}\,\mathrm{F.m}^{-1}$ is the permittivity of vacuum. Note that we use S.I. units in these definitions, but choose to absorb the factor ε_0 in the definition of the polarisability α_i, defined in Eq. S15, and therefore expressed in units of $[\mathrm{F.m}^2]$. For an isotropic response, α_i is simply the molecular polarisability. For a general polarisability tensor, $\mathbb{\alpha}$, and a random orientation of molecules (as in a gas or a solution), α_i is an effective polarisability representing the orientation-averaged response and is given by

$$\alpha_i = \frac{1}{3}\mathrm{Tr}(\mathbb{\alpha}) = \frac{\alpha_{xx} + \alpha_{yy} + \alpha_{zz}}{3}. \tag{S2}$$

The polarisability tensors considered in the main manuscript for coupled-dipole simulations are either isotropic,

$$\mathbb{\alpha} = \begin{pmatrix} \alpha_i & 0 & 0 \\ 0 & \alpha_i & 0 \\ 0 & 0 & \alpha_i \end{pmatrix} \tag{S3}$$

or uniaxial,

$$\mathbb{\alpha} = \begin{pmatrix} 0 & 0 & 0 \\ 0 & 0 & 0 \\ 0 & 0 & 3\alpha_i \end{pmatrix}; \tag{S4}$$

these tensors are expressed in their natural frame (where they are diagonal), and need to be rotated appropriately for the specific molecular orientations presented in Fig. 4.

In the effective-medium model of Sec. 1 the shell is composed of a mixture of water and dye molecules. Pure water has a refractive index of $\sqrt{\varepsilon_w} = 1.33$, which using Eq. S1 yields $\bar{\alpha}_w = 0.204$. The dye molecule is characterized by an effective polarisability α_d as defined in Eq. S2, so $\bar{\alpha}_d = \frac{c_d \alpha_d}{3\varepsilon_0}$, where c_d is the dye concentration in m^{-3}. Solving Eq. S1 for ε, the

mixture's dielectric function now explicitly depends on dye concentration:

$$\varepsilon_{\text{shell}}(c_d) = \frac{1 + 2(\bar{\alpha}_w + \frac{c_d \alpha_d}{3\varepsilon_0})}{1 - (\bar{\alpha}_w + \frac{c_d \alpha_d}{3\varepsilon_0})}. \tag{S5}$$

We take the following model (lorentzian) to describe the microscopic polarisability α of a molecule in a vacuum,

$$\alpha_d = \alpha_\infty + \frac{\alpha_1 \lambda_1}{\mu_1} \left[\frac{1}{1 - \frac{\lambda_1^2}{\lambda^2} - i\frac{\lambda_1^2}{\lambda \mu_1}} - 1 \right] \tag{S6}$$

For a simplified model of a dye resembling Rhodamine 6G, we use $\alpha_\infty = 3.2 \times 10^{-39}\,[\text{SI}]$, $\alpha_1 = 1.92 \times 10^{-38}\,[\text{SI}]$, $\lambda_1 = 526\,\text{nm}$, $\mu_1 = 10^4\,\text{nm}$. We emphasize that for the concentration-dependence to be meaningful the magnitude of α_d must be correct. In many studies, this is freely adjusted to match experimentally-observed spectral shifts. Here, we instead use the experimentally measured absorption cross-section to determine the absolute α_d, as discussed in Ref. 3. Taking into account the local-field enhancement of the solvent (of refractive index $n = \sqrt{\varepsilon_w}$), the absorption cross-section of an isolated dye in water is given by[3,4]

$$\sigma_{\text{abs}}(\lambda) = \frac{2\pi}{\lambda \varepsilon_0 \sqrt{\varepsilon_w}} L_w^2 \text{Im}\left(\alpha_d(\lambda)\right) \tag{S7}$$

with the local field factor

$$L_w = \frac{\varepsilon_w + 2}{3}, \tag{S8}$$

and α_d defined in Eq. S2 in the generic anisotropic case.

A.2 Link between Eqs. S5 and S7

Eq. S7 can be derived from the orientation-averaged microscopic response of the dye in solution, corrected by local field effects due to the solvent.[4] To give further support to our derivation of Eq. S5, we here show that Eq. S7 can be derived from it.

We consider a dilute solution of dyes in water and will derive the absorption cross-section using a macroscopic description using the dielectric function given by Eq. S5. The absorption coefficient in a medium of complex refractive index $\sqrt{\varepsilon}$ is given by $\kappa = (4\pi/\lambda)\text{Im}(\sqrt{\varepsilon})$, from which the absorption cross-section for a single dye is simply obtained as $\sigma_{\text{abs}} = \kappa / c_d$.

For a dilute solution, we can assume that $\bar{\alpha}_d \ll \bar{\alpha}_w$, and find the first order expansion of Eq. S5 in terms of $\bar{\alpha}_d$. After some manipulation, and substituting $\bar{\alpha}_w$ with $(\varepsilon_w - 1)/(\varepsilon_w + 2)$, we obtain

$$\varepsilon \approx \varepsilon_w \left[1 + \frac{2\bar{\alpha}_d}{1 + 2\bar{\alpha}_w} \frac{\bar{\alpha}_d}{1 - \bar{\alpha}_w}\right] \tag{S9}$$

$$\approx \varepsilon_w \left[1 + \frac{\bar{\alpha}_d(\varepsilon_w + 2)^2}{3\varepsilon_w}\right] \tag{S10}$$

from which we deduce

$$\sqrt{\varepsilon} \approx \sqrt{\varepsilon_w} \left[1 + \frac{3\bar{\alpha}_d L_w^2}{2\varepsilon_w}\right] \tag{S11}$$

and writing $\bar{\alpha}_d = \alpha_d c_d/(3\varepsilon_0)$:

$$\kappa = \frac{4\pi}{\lambda}\mathrm{Im}(\sqrt{\varepsilon_w}) \approx \frac{2\pi L_w^2}{\lambda\varepsilon_0\sqrt{\varepsilon_w}}\mathrm{Im}(\alpha_d)c_d \tag{S12}$$

$\sigma_{\mathrm{abs}} = \kappa/c_d$ then yields Eq. S7.

A.3 Model comparison in the low concentration limit

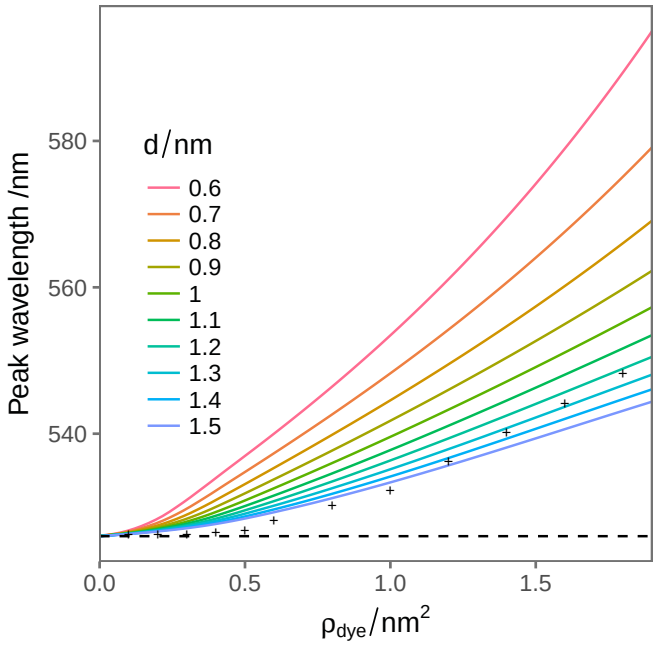

Figure S1: Effect of the shell thickness on the predicted spectral shifts in the low concentration limit. The solid lines present the results for effective-medium calculations with varying value of shell thickness d. The points correspond to the spectral shifts predicted by the coupled dipole model with isotropic dipoles presented in Fig. 2b.

In the low-concentration limit, Eq. S10 indicates that

$$\varepsilon - \varepsilon_w \approx 1 + c_d \frac{(\varepsilon_w + 2)^2}{9\varepsilon_0} \alpha_d \tag{S13}$$

At low dye concentrations we may assume that the electric field in the shell is not strongly affected from its value E_0 in the surrounding medium by the dye molecules; the total absorption is given by

$$\iiint_{\text{volume}} \Im\left(\varepsilon_{\text{shell}}\right) |E|^2 \, dV \approx c_d \frac{L_w^2}{\varepsilon_0} \Im\left(\alpha_d\right) \times d(4\pi R^2) |E_0|^2, \tag{S14}$$

where we approximated the volume of the thin shell by $d(4\pi R^2)$ and assumed a constant field across the nanoshell volume. We can therefore conclude that varying the thickness d for a given number of dyes (surface coverage ρ_d) has no net effect (for small variations), as the volume concentration $c_d \propto 1/d$, while the volume scales with d. The predicted absorption from the effective-medium shell model is therefore independent on the shell thickness at low surface coverage, and proportional to ρ_d.

We present in Fig. S1 further evidence of this in a comparison of peak absorption wavelength against surface coverage for homogeneous shell model calculations with varying shell thickness d. All the curves approach the same value as $\rho_d \to 0$, which correspond to the unperturbed dye absorption peak (526 nm) in water. The peak intensities also coincide, when normalised to the effective number of dyes (not shown). This first-order behaviour in dye concentration validates our use of the Clausius-Mossotti formula in the effective-medium shell model.

Figure S1 also presents for comparison the peak positions retrieved from Fig. 2b in the main manuscript, namely for isotropic point dipoles at corresponding surface coverage. The low-coverage limit agrees with the effective-medium simulations and coincides with the response of an isolated dye in the medium, when intensities are scaled by the number of dipoles. It is interesting to note however that the discrete point dipole model predicts a different trend for the spectral shift at larger concentrations than any of the effective-medium models with a fixed effective thickness d. This highlights a clear limitation of this effective-

medium theory to account for the optical response of what is intrinsically a non-homogeneous, and non-bulk, system. Low coverage corresponds to few discrete dipoles arranged around a sphere, and their specific position, whether well-separated, or clustered, depending on the chosen adsorption model, will lead to weaker or stronger averaged interactions between neighbours. For the homogeneous coverage considered in Fig. 2b the dipoles are relatively far apart on the surface of a 15 nm-radius sphere, yielding a small spectral shift compared to the effective-medium predictions that assume homogeneously-distributed dipoles in bulk.

B Coupled dipole equations

We summarise below the standard equations of coupled-dipole theory, as no single convention exists for the various prefactors affecting the definition of polarisability and other quantities.

We consider a collection of N point electric dipoles $\mathbf{p}_i$ located at $\mathbf{r}_i$ and embedded in a homogeneous infinite medium characterised by a dielectric function ε_w. The dipoles are subject to an incident macroscopic field $\mathbf{E}_{\text{inc}}$. The response of the point dipoles $\mathbf{p}_i$ is assumed local and linear and described by a polarisability tensor (possibly different for each molecule) as:

$$\mathbf{p}_i = \mathbb{\alpha}_i \mathbf{E}_i, \tag{S15}$$

At a microscopic level, a dipole reacts to the applied field with an intrinsic polarisability α^μ. The applied field is enhanced by a local-field correction L_w arising from the polarisation of the embedding medium (Eq.S8). In turn, such a dipole moment produces a field which is enhanced by the same local field factor, from a reciprocity argument. We may therefore define an effective macroscopic polarisability α as

$$\alpha = L_w^2 \alpha^\mu. \tag{S16}$$

The macroscopic electric field created by such a dipole $\mathbf{p}_i$ at a general point $\mathbf{r}$ also depends linearly on that dipole moment,

$$\mathbf{E}_{\mathbf{p}_i}(\mathbf{r}) = \mathbb{G}(\mathbf{r}_i, \mathbf{r})\, \mathbf{p}_i, \tag{S17}$$

where the Green's tensor $\mathbb{G}$ characterises the electric field at $\mathbf{r}$ created by a unit point dipole at $\mathbf{r}_i$.

A given dipole responds to a net macroscopic field that is the sum of the incident field and the field scattered by its neighbours. With the above conventions, the coupled dipole equations take the form,

$$\mathbf{p}^i = \alpha_i \left(\mathbf{E}_{\text{inc}}(\mathbf{r}_i) + \sum_{j \neq i} \mathbb{G}_{ij} \mathbf{p}^j \right), \tag{S18}$$

where $\mathbf{E}_{\text{inc}}(\mathbf{r}_i)$ is the incident field, and $\mathbb{G}_{ij} = \mathbb{G}(\mathbf{r}_i, \mathbf{r}_j)$ is the Green's tensor for the field created by dipole j at the location of dipole i in the infinite surrounding medium,

$$\mathbb{G}_{ij} = \beta^{-1} \frac{e^{ik_1 r}_{ij}}{r_{ij}} \left\{ k_1^2 \left[\mathbb{I} - \hat{\boldsymbol{r}}_{ij} \otimes \hat{\boldsymbol{r}}_{ij} \right] - \left(\frac{1}{r_{ij}^2} - \frac{ik_1}{r_{ij}} \right) \left[\mathbb{I} - 3\hat{\boldsymbol{r}}_{ij} \otimes \hat{\boldsymbol{r}}_{ij} \right] \right\} \tag{S19}$$

where k_1 is the wave vector in the embedding medium, and we introduced the prefactor $\beta = 4\pi\varepsilon_0\varepsilon_w$ which may be simplified throughout in practice by defining suitably-normalised quantities.

The absorption cross-section is given by:

$$\sigma_{\text{abs}} = \frac{4\pi\beta k_1}{|E_0|^2} \sum_i \left(\Im \left[\mathbf{p}_i \cdot \mathbf{E}_i^* \right] - \frac{2\beta}{3} k_1^3 |\mathbf{p}_i|^2 \right). \tag{S20}$$

C Consistency of results with random orientations

In Fig. 4c of the main manuscript the molecules assume a random in-plane orientation on the spherical surface. Each coupled-dipole simulation will therefore produce different results, but we show in Fig. S2 that the variations are minimal and do not affect our conclusions. That the spectral lineshape (shift and broadening of the absorption line) due to the dipole-dipole interactions is so reproducible, even for two different realisations of a disordered cluster of

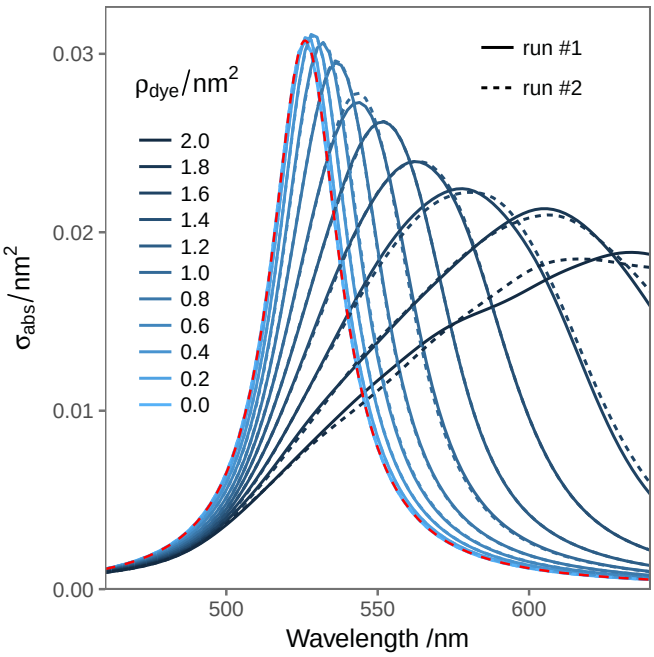

Figure S2: Comparison of two sets of simulations for the configuration discussed in Fig. 4c of the main manuscript. Dipoles with uniaxial polarisability tensors are oriented tangentially, but with random in-plane orientation. The solid and dashed curves show the predicted spectra for two sets of simulations (each individual curve corresponds to a specific cluster realisation, for a given concentration). The results are very similar, especially at low concentrations. Small variations of the order of a few percent are observed in absolute intensities, but the lineshape evolution is very consistent.

dipoles, is due to a combination of two factors. Firstly, the simulations involve a relatively large number of dipoles, from a few hundreds to a few thousands in this case. Secondly, the cross-sections are averaged over all orientations of incident light and polarisations. Both aspects contribute to an averaging of the response, smoothing out any particular differences between individual pairwise dipole interactions.

D Shell radius dependence

For practical reasons the simulations were performed for a 15 nm radius sphere; this arbitrary choice was made to limit the maximum number of dipoles in a given simulation to a few thousands, so that solving the resulting $3N \times 3N$ linear system of coupled-dipole equations remain manageable on a standard desktop computer. We performed test simulations at other sizes, and found little variation in the 10–50 nm size range (shell radius), corresponding to many typical nanoparticles. Such supplementary calculations are presented in Fig. S3 for two different situations. In panel (a) we used Mie theory and the effective-medium approximation to predict the radius-dependence of the absorption cross-section, at a fixed surface coverage $\rho = 2\,\mathrm{nm}^{-2}$, with no computational difficulties. The lineshape shows very little variation (and even beyond this size range, not shown here). The bottom panel (b) presents coupled-dipole simulations for varying radii of curvature in the range 15–30 nm. Here, due to limitations in computational resources, we did not model a full spherical shell but only a spherical cap with surface area 20% of the full sphere. This constraint limited the maximum number of dipoles, while allowing the radius of curvature, and therefore the relative position of neighbouring dipoles, to be varied. We confirmed on the smaller sphere that the predictions for a spherical cap and a full spherical surface differ only slightly, no more than the variation due to the radius in this figure. Together, both results confirm the validity of our predictions for a broad range of nanoshells, although of course for a fully-quantitative prediction of spectral shifts in a specific configuration the exact position of all the dipoles should be taken into account (but in realistic comparisons with experiments, these are unlikely to be available).

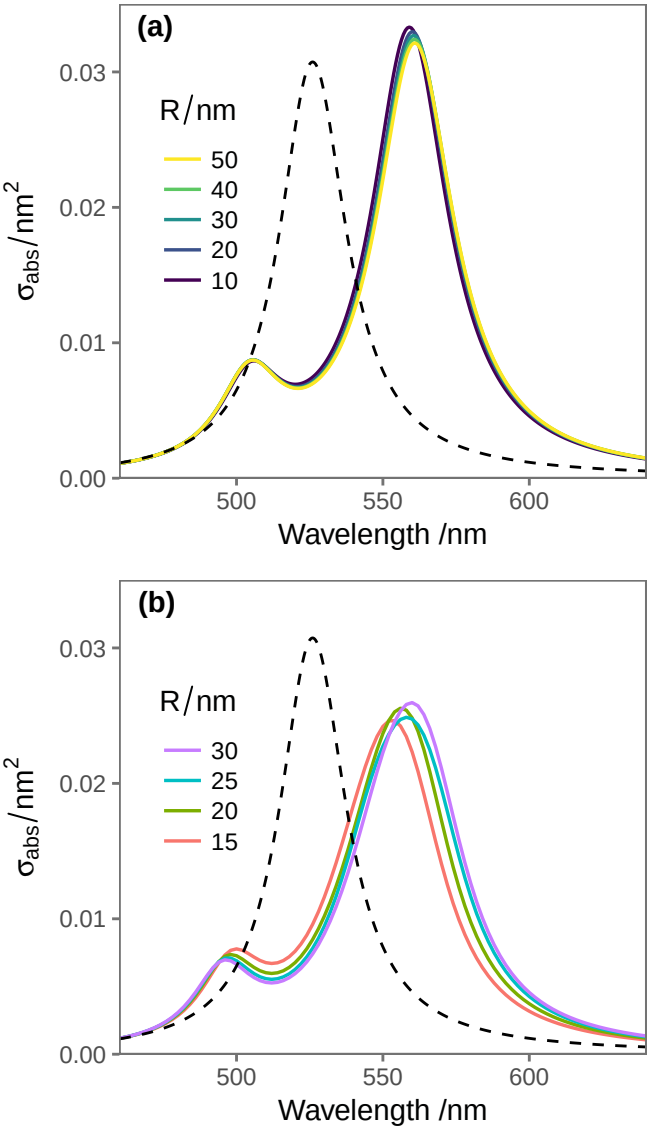

Figure S3: Effect of sphere radius on the predicted absorbance spectra. (a) Mie theory simulations for shells of thickness $d = 1\,\mathrm{nm}$ with varying radius, using an effective-medium dielectric function with concentration-equivalent surface coverage $\rho = 2\,\mathrm{nm}^{-2}$. (b) Coupled-dipole simulations for isotropic dipoles homogeneously distributed on a spherical patch with varying radius of curvature. The dipole density is kept constant at $\rho = 2\,\mathrm{nm}^{-2}$, and the number of dipoles is increased with the radius, covering 20% of the full spherical surface in order to reduce the total number of dipoles in the simulations. As in all the figures, the cross-sections are normalised by the number of dipoles.

References

(1) Aspnes, D. E. Optical properties of thin films. *Thin Solid Films* **1982**, *89*, 249–262.

(2) Markel, V. A. Introduction to the Maxwell Garnett approximation: tutorial. *JOSA A* **2016**, *33*, 1244–1256.

(3) Djorović, A.; Meyer, M.; Darby, B. L.; Le Ru, E. C. Accurate modeling of the polarizability of dyes for electromagnetic calculations. *ACS Omega* **2017**, *2*, 1804–1811.

(4) Le Ru, E. C.; Etchegoin, P. G. *Principles of surface enhanced Raman spectroscopy and related plasmonic effects*; Elsevier: Amsterdam, 2009.